

**Conformational Coupling Across
the Plasma Membrane
in Activation of the EGF receptor**

Nicholas F Endres^{1,3+}, Rahul Das^{1,3+}, Adam Smith^{2,5+}, Anton Arkhipov⁶, Erika Kovacs^{1,3},
Yongjian Huang^{1,3}, Jeffrey G. Pelton³, Yibing Shan⁶, David E. Shaw^{6,7},
David E. Wemmer^{2,3,5}, Jay T. Groves^{2,3,4,5*} and John Kuriyan^{1,2,3,4,5*}

+ These authors made equal contributions.

* To whom correspondence should be addressed:

John Kuriyan: kuriyan@berkeley.edu

Jay T. Groves: jtgroves@lbl.gov

¹Department of Molecular and Cell Biology

²Department of Chemistry

³California Institute for Quantitative Biosciences

⁴Howard Hughes Medical Institute, University of California, Berkeley, CA, 94720, USA

⁵Physical Sciences Division, Lawrence Berkeley National Laboratory, Berkeley, CA, 94720, USA

⁶D.E. Shaw Research, New York, NY 100036

⁷The Center for Computational Biology and Bioinformatics, Columbia University, New York, NY, 10032

Summary

How the epidermal growth factor receptor (EGFR) activates is incompletely understood. The intracellular portion of the receptor is intrinsically active in solution, and to study its regulation we measured autophosphorylation as a function of EGFR surface density in cells. Without EGF, intact EGFR escapes inhibition only at high surface densities. While the transmembrane helix and the intracellular module suffice for constitutive activity at low densities, the intracellular module is inactivated when tethered on its own to the plasma membrane and fails to dimerize, as determined by fluorescence cross-correlation spectroscopy. NMR and functional data indicate that activation requires an N-terminal interaction between the transmembrane helices, which promotes an antiparallel interaction between juxtamembrane segments and release of inhibition by the membrane. We conclude that EGF binding removes steric constraints in the extracellular module, allowing activation through N-terminal association of the transmembrane helices.

Introduction

In receptor tyrosine kinases, such as the epidermal growth factor receptor (EGFR), a single transmembrane helix connects an N-terminal and extracellular ligand-binding module to an intracellular tyrosine kinase domain (Hubbard and Till, 2000; Lemmon and Schlessinger, 2010). Ligand binding leads to increased catalytic activity in the kinase domains and phosphorylation of intracellular tyrosine residues in the receptors or in associated proteins. In EGFR, these tyrosines are located mainly in a long C-terminal tail, and when phosphorylated, they serve as docking sites for diverse signaling proteins (Scott and Pawson, 2009). Aberrant activation of receptor tyrosine kinases is implicated in many diseases, particularly cancer, underscoring their critical role in regulating metabolism, growth and differentiation (Cohen, 2002; Hynes and Lane, 2005).

In this paper, and a companion one (Arkhipov et al.), we examine how ligand binding to the extracellular module of EGFR activates its kinase domains. EGFR was the first growth-factor receptor demonstrated to undergo ligand-dependent dimerization (Yarden and Schlessinger, 1987), and crystal structures have shown how ligand binding promotes the dimerization of the extracellular module (Ferguson et al., 2003; Garrett et al., 2002; Ogiso et al., 2002). A critical step in EGFR activation is the formation of an asymmetric dimer of kinase domains (Zhang et

al., 2006). In this asymmetric dimer, the C-terminal lobe of one kinase domain (the activator) and the N-terminal lobe of another kinase domain (the receiver) associate, stabilizing an active conformation of the receiver kinase domain (Zhang et al., 2006). Activation through asymmetric homo- or hetero-dimerization is also utilized by the three close relatives of EGFR: Her2, Her3 and Her4 (Jura et al., 2009b; Qiu et al., 2008; Shi et al., 2010) (also known as ErbB2, ErbB3, ErbB4), and underlies the combinatorial activation of EGFR family members. In particular, Her3, which has a catalytically impaired kinase domain, is a potent activator of Her2, which has no ligand for its extracellular domain (Wallasch et al., 1995).

It is natural to think that ligand-driven dimerization simply converts inactive monomers into active dimeric receptors. The mechanism for ligand-dependent activation must, however, be more complex because the intracellular module of the receptor (consisting of the juxtamembrane segment, kinase domain and C-terminal tail) is capable of dimerizing and activating on its own (Jura et al., 2009a; Red Brewer et al., 2009; Thiel and Carpenter, 2007). The ability of the isolated intracellular module to dimerize and activate in solution is a consequence of the juxtamembrane segments functioning as a latch, holding the kinase domains in the asymmetric configuration necessary for activity (Jura et al., 2009a; Red Brewer et al., 2009). There are two

parts to this interaction. The C-terminal portion of the juxtamembrane segment (denoted JM-B) of the receiver kinase latches on to the activator kinase domain (Figure 1A). The N-terminal portion of the juxtamembrane segment (JM-A) forms an antiparallel helical association between subunits, further stabilizing the asymmetric dimer (Jura et al., 2009a; Scheck et al., 2012). Clearly, the responsiveness of the receptor to ligand implies that the intrinsic ability of the intracellular module to activate is suppressed in some way when the ligand is not bound.

EGFR family members are also prone to ligand-independent dimerization and activation, particularly at high expression levels (Nagy et al., 2010). Ligand-independent dimerization may be facilitated by the fact that the dimer interface for these receptors, are formed entirely by the receptors themselves, with no contribution from the ligand (Garrett et al., 2002; Ogiso et al., 2002). The coupled equilibria governing EGFR activation, incorporating both ligand-independent and ligand-dependent dimerization, are diagrammed in Figure 1A (Yarden and Schlessinger, 1987). This diagram omits the formation of higher-order oligomers (Clayton et al., 2008) and negative cooperativity in ligand binding (Alvarado et al., 2010; Liu et al., 2012; Macdonald and Pike, 2008), both of which are also likely to be important for EGFR function.

We now present the results of a combined experimental and simulation study aimed at understanding how the conformations of the extracellular and intracellular module are coupled. We present our findings in two papers. This paper describes experimental analyses of EGFR activation, while the companion paper presents the results of molecular dynamics simulations of the receptor in lipid bilayers (Arkhipov et al.). We refer to these simulations often in this paper since they provide a framework for discussing the experimental results.

In this paper we begin by comparing the activity of full-length EGFR to that of two constructs, one lacking the extracellular module (including only the transmembrane helix and the intracellular module), and the other containing just the intracellular module fused to the membrane-localization motif of c-Src. All of these constructs activate at higher levels of expression, so to compare them in a meaningful way we used immunofluorescence to measure EGFR autophosphorylation as a function of receptor surface density in cells. Our data lead to the unexpected conclusion that the intrinsic activity of the intracellular module is inhibited when it is tethered to the plasma membrane. We used fluorescence cross-correlation spectroscopy (FCCS) to study the oligomerization of various EGFR constructs, and found that the inhibition of the intracellular module at the membrane is due to a failure to dimerize. These data point to a critical

role for the transmembrane helix in dimerizing and activating the intracellular module, but the role of the transmembrane helix in EGFR activation is poorly understood (Lu et al., 2010; Moriki et al., 2001). We address this issue in the final part of this paper, in which we present an analysis by NMR of the transmembrane and juxtamembrane segments of EGFR, embedded in lipid bilayers.

!

Results and Discussion

Ligand-independent activation of EGFR depends on the surface density of the receptor and formation of the asymmetric dimer

An essential part of our analysis is to determine the activity of the receptor as a function of its surface density. Cos-7 cells were transiently transfected with various EGFR constructs, which results in different expression levels in individual cells. EGFR levels and phosphorylation at a specific residue in the C-terminal tail (Tyr 1068) were monitored on a cell-by-cell basis by fusing constructs to the fluorescent protein mCherry and using a phosphospecific primary antibody and a fluorescein-labeled secondary antibody, respectively (Figure 2A and Experimental Procedures).

We first present immunofluorescence data for full-length EGFR that define the range of surface densities at which the receptor is most responsive to ligand. We stimulated with saturating levels of EGF for short times (3-5 minutes) to minimize internalization (Sorkin and Goh, 2009). Due to the morphology of Cos-7 cells, which resembles that of a fried egg, we could

focus our analysis on plasma-membrane localized EGFR by selecting regions at the periphery of the cells (Figure S3). We calibrated our microscope so that we could relate the fluorescence intensity of EGFR in these peripheral regions to its surface density (Galush et al., 2008). In this way, we obtain a cell-by-cell quantification of the relative tyrosine phosphorylation level as a function of the surface density of EGFR at the plasma membrane (Figure S1A).

The dependence of EGFR activation on surface density, averaged over many cells (~ 100), is shown in Figure 2B for Tyr 1068. When we normalize the data to represent the relative phosphorylation level per molecule as a function of surface density (right panel, Figure 2B), we observe that EGF-stimulated phosphorylation is independent of the receptor surface density, over the experimental range considered (50-2000 receptors per μm^2). This indicates that EGF binding is sufficient to trigger the formation of the asymmetric interaction between kinase domains and any higher order structures necessary for phosphorylation, even at the lowest surface densities observed in our study.

In the absence of EGF, the relative phosphorylation level per receptor increases with receptor surface density, reaching values at the highest densities that are comparable to those obtained upon EGF stimulation. At a surface density of ~ 1400 receptors per μm^2 , the mean

phosphorylation level of the unliganded receptor is roughly half of that observed when EGF is added (Figure 2B). If we assume that the kinase domains of the receptor are constrained to a ~10 nm-thick shell at the plasma membrane, then a surface density of 1400 receptors per μm^2 is equivalent to a local concentration of kinase domains of ~200 μM (Extended Experimental Procedures), ~100-fold higher than that required for robust activation of the intracellular module in solution (Jura et al., 2009a).

The level of EGF-independent phosphorylation of the receptor is essentially the same as the EGF-induced level when the surface density of the receptor becomes higher than ~2000 receptors per μm^2 . This corresponds to ~1.3 million receptors per cell, assuming a 10 μm radius for the average cell used in our study (Extended Experimental Procedures). This is comparable to the levels of EGFR expression reported in cancer cells that overexpress EGFR (Haigler et al., 1978), consistent with the known role of overexpression of the receptor in cancer development (Hynes and Lane, 2005).

EGF-independent activation at high expression levels is not simply due to spontaneous transphosphorylation through a nonspecific mechanism, because it requires formation of the asymmetric dimer. Introduction of the V924R mutation, which disrupts the interface between

the activator and receiver kinases in the asymmetric dimer and is located far from the active site (Zhang et al., 2006), completely suppresses ligand-independent EGFR activity in the range of surface densities examined (Figure S1C). There is a modest increase in phosphorylation level upon EGF treatment in cells expressing the V924R mutant, but this increase is independent of surface density, and is probably due to low levels of endogenous EGFR.

A similar dependence of phosphorylation level on surface density is seen when other tyrosine residues are monitored (such as Tyr 1173, Figure S1B). We observe the same general pattern when we examine these cells using fluorescence-activated cell sorting (FACS), with formation of the asymmetric dimer being required (Figure S1D). Since FACS analysis does not provide an easy way to distinguish between expression of constructs at the cell surface and on internal membranes, we focus primarily on results from immunofluorescence microscopy.

The extracellular module blocks receptor activation in the absence of ligand

It is well known that deletion of the extracellular module activates EGFR, although it is not clear if this effect is restricted to high levels of receptor expression (Chantry, 1995; Nishikawa et al., 1994; Zhu et al., 2003). To address this, we measured phosphorylation as a function of

surface density for a construct of EGFR, in which the extracellular module is deleted, leaving just the transmembrane helix and the intracellular module (TM-ICM, Figure 1B, 2C).

The TM-ICM construct does not localize solely to the plasma membrane, with more protein concentrated in internal membranes than seen for comparable expression levels of intact EGFR (Figure S1E). Nevertheless, by focusing on the peripheral regions in these cells, we find that phosphorylation of TM-ICM at the plasma membrane is much greater than for the unliganded receptor, even at the lowest surface densities studied (Figure 2C). Like the EGF-activated receptor, the normalized phosphorylation level of TM-ICM does not depend on its surface density, consistent with constitutive activation.

To test the importance of the linkage between the extracellular module and the transmembrane helix, we inserted a flexible linker consisting of twenty glycine, serine and threonine residues between them (ECM-GlySer-TM-ICM, Figure 1B). The ECM-GlySer-TM-ICM construct shows a substantial increase in ligand-independent phosphorylation at low receptor densities compared to the wildtype receptor (Figure 2D). This observation is consistent with a previous study in which the insertion of a larger and less flexible linker between the extracellular module and the transmembrane helix increased ligand-independent activation of the

receptor in cells overexpressing EGFR (Sorokin, 1995). In contrast to the TM-ICM construct, the localization of ECM-GlySer-TM-ICM is indistinguishable from that of the wild-type receptor (Figure S1E), adding confidence to our inference that the extracellular module inhibits EGFR activity in the absence of ligand by preventing spontaneous formation of the asymmetric interaction between kinase domains.

The intracellular module of EGFR is inhibited at the plasma membrane

To test the role of the transmembrane helix in activation, we generated a construct in which the extracellular module and the transmembrane helix are both deleted. This construct (Myr-ICM) has the intracellular module fused to a plasma membrane-targeting motif derived from c-Src (Reuther et al., 2000; Silverman and Resh, 1992), which take the place of the transmembrane helix.

Given the high activity of the intracellular module in solution (Jura et al., 2009a), and previous suggestions that the transmembrane helix is likely to play a passive role in coupling to the extracellular module (Lu et al., 2010), we expected that localization of the intracellular module alone to the plasma membrane would result in robust autophosphorylation, due to the

substantial enhancement in its local concentration over the solution concentrations required for activity. Surprisingly, confocal images clearly show that Myr-ICM is strongly inhibited on the plasma membrane. Even cells with high levels of Myr-ICM localized to the plasma membrane show low levels of phosphorylation when compared to the EGF-treated full-length receptor at much lower expression levels (Figure 3A). Analysis of the surface-density dependence of Myr-ICM activation confirms that this construct is inhibited substantially relative to EGF-treated EGFR (Figure 3B).

The intracellular domain can be activated constitutively at the plasma membrane by the insertion of the coiled-coil segment from the transcription factor GCN4 (O'Shea et al., 1991) between the c-Src membrane-localization motif and the intracellular module (Myr-GCN4-ICM, Figure 1B), which presumably enforces dimerization (Figure 3B). In contrast, a construct in which a flexible linker (GGGTGGGS) is inserted between the c-Src motif and the juxtamembrane segment exhibited low activity (Figure S2A), indicating that direct interference by the c-Src motif is unlikely to be responsible for the inhibition of Myr-ICM.

Molecular dynamics simulations of inactive and unliganded EGFR (Arkhipov et al.) suggest two reasons for inhibition of the intracellular module at the membrane (Figure 3C). First, the JM-

A segment interacts tightly with the membrane, and the antiparallel association between JM-A segments cannot occur because the three leucine sidechains at the heart of this interface (located within an LRLL motif) are buried in the hydrophobic part of the membrane. Second, negatively charged lipids in the membrane interact extensively with positively charged sidechains in the kinase domain and the juxtamembrane segment. These observations lend support to previous speculations that such interactions may inhibit the receptor (McLaughlin et al., 2005).

Many of the membrane-interacting elements are important for activation and substrate binding, so it is difficult to design mutations that would weaken interactions between the intracellular module and the plasma membrane without compromising function. We focused on four lysine residues in the N-terminal lobe of the kinase domain (residues 689, 692, 713 and 715) that do not appear to be involved in the formation of the asymmetric dimer, but are seen to interact with the membrane in the simulations. Replacement of two of these residues at a time with glutamate results in substantial activation of the Myr-ICM construct in the single-cell assay (Myr-ICM K713E/K715E and Myr-ICM K689E/K692E, Figures 3D,E), without affecting membrane localization as judged by confocal imaging (Figure S2B).

Introduction of the same mutations in the context of the full-length receptor does not result in enhanced phosphorylation in the single-cell assay or in the FACS analysis (data not shown). Thus, while our data support the idea that electrostatic interactions between the kinase domain and the plasma membrane are inhibitory, it appears that other inhibitory interactions with the membrane, such as those involving the JM-A segment, and the steric block provided by the extracellular module, are dominant.

To test if the kinase domain is inhibited within the context of the full-length receptor, we replaced the 12 residues in the JM-A segment by a flexible linker consisting of three repeats of the motif Gly-Gly-Gly-Ser (ECM-TM-GlySer-ICM, Figure 1B). This construct retains the JM-B segment, which stabilizes the active asymmetric dimer by forming the “juxtamembrane latch”. In solution, the presence of the JM-B segment activates the kinases at concentrations of $\sim 10 \mu\text{M}$ (Jura et al., 2009a), which is at the low-end of the effective concentrations we observe for the receptor on the plasma membrane ($10\text{-}300 \mu\text{M}$). The ECM-TM-GlySer-ICM construct is strongly inhibited both in the absence and presence of EGF at densities as high as 2000 molecules per μM^2 (or $\sim 300 \mu\text{M}$ effective concentration) (see Figure 3F), consistent with the

idea that inhibitory interactions between the kinase domains and the plasma membrane play a role in preventing ligand-independent activation.

The intracellular module is predominantly monomeric at the plasma membrane

These results led us to wonder if dimerization of the intracellular module is prevented at the plasma membrane. In order to assess the level of oligomerization of various EGFR constructs in live cells, we used two-color pulsed-interleaved excitation fluorescence cross-correlation spectroscopy (PIE-FCCS), in which a pair of lasers alternately excites GFP and mCherry with sub-nanosecond pulses (Muller et al., 2005) (Figure 4A). Diffusion of individual molecules in and out of the diffraction-limited laser focus gives rise to fluorescence-intensity fluctuations that have a characteristic time scale, directly related to the mobility of the molecules. If GFP and mCherry-tagged molecules enter and leave the laser focus together, then there will be correlated fluorescence-intensity fluctuations in the GFP and mCherry detection channels. By analyzing these fluctuations we calculate a cross-correlation value, which is proportional to the fraction of co-diffusing molecules (Larson et al., 2005) (Figure S4A).

The observation of correlated diffusion with PIE-FCCS is a rigorous indicator of molecular association and is not affected by random, dynamic collisions and crowding effects that complicate FRET-based assays. An advantage of PIE-FCCS when compared to conventional FCCS is that photons are detected individually and their arrival times are recorded with 32 ps precision using a routed two-channel time correlated single photon counting module (Becker et al., 2005). This enables unambiguous assignment of each detected photon to an excitation laser source, ensuring that any cross correlation we observe is due to co-diffusion and not spectral cross-talk (Figure S4B, Extended Experimental Procedures) (Muller et al., 2005).

We used PIE-FCCS to measure cross-correlation values for co-expression of various EGFR constructs fused to GFP or mCherry (Figure 4B). Measurements were made at the cell periphery, and we explicitly avoided large ($>1\ \mu\text{m}$), high intensity features. We restricted our analysis to cell densities ranging from 100-1000 molecules per μm^2 , the range of densities in which ligand-independent activation of EGFR is strongly inhibited.

To determine the extent to which Myr-ICM dimerized, we compared its cross-correlation values to that of the Myr-GCN4-ICM construct, which is constitutively active (Figure 3B) and presumably dimerized by the GCN4 coiled-coil. The cross-correlation values for Myr-ICM are

significantly lower than for Myr-GCN4-ICM, demonstrating that the addition of GCN4 substantially increases the propensity of Myr-ICM to self-associate. The cross-correlation values for Myr-ICM are comparable to those for a monomeric control, in which GFP and mCherry, each fused to the c-Src localization sequence, are coexpressed (Figure 4C). The cross-correlation value for Myr-GCN4-ICM is roughly half that obtained for a fusion of GFP and mCherry in one protein (Figure S4C), consistent with it being a dimer (in a random population of dimers, 50% should be GFP, mCherry pairs). Differences in cross correlation between Myr-ICM and Myr-GCN4-ICM do not change significantly over the range of densities we observe (100-1000 molecules per μm^2) (Figure S4D). While the precise oligomeric state cannot be determined from cross-correlation values, our results demonstrate that Myr-ICM oligomerization is inhibited relative to that of Myr-GCN4-ICM on the plasma membrane, and that it is likely to be monomeric over the range of surface densities examined.

The cross-correlation values for unliganded full-length EGFR are similar to those for the monomeric controls, indicating that the intact receptor is also predominantly monomeric in the same range of surface densities for which ligand-dependent activation is suppressed (less than 1000 receptors per μm^2). Treatment with saturating levels of EGF significantly increases cross-

correlation values, indicating that EGF binding increases the oligomeric state of the receptor. This EGF-induced increase in clustering does not depend on the kinase activity of the receptor (Figure S4E). The cross-correlation values for EGF-stimulated EGFR are, on average, less than expected for a constitutive dimer, based on comparison to Myr-GCN4-ICM. This may be due a reduction in the ability of EGF to access EGFR on the basal membrane, which is adhered to the glass surface. This is suggested by confocal images, in which phosphorylation of Tyr1068 in EGF-treated cells is stronger on the apical membrane (Figure 3A). Our results are consistent with a monomer-to-dimer transition driving EGFR activation at low surface densities.

Structural analysis of the transmembrane and the juxtamembrane segments in lipid bilayers

The data presented thus far point to a critical role for the transmembrane helix because its presence is sufficient to convert the inactive intracellular module to an active form at low surface densities. In order to understand the structural basis for this, we used NMR to analyze a fragment of EGFR spanning the transmembrane helix and the first 29 residues of the juxtamembrane segment (TM-JM, residues 618 - 673). We reconstituted the TM-JM construct

into lipid bilayers in the form of bicelles made from 1,2-dimyristoyl-sn-glycero-3-phosphocholine (DMPC) and 1,2-dihexanoyl-sn-glycero-3-phosphocholine (DHPC). These bicelles, in which the DMPC lipids form a bilayer around which the shorter DHPC lipids form a collar, have been used previously to analyze the transmembrane helices of EGFR and HER2 (Bocharov et al., 2008; Mineev et al., 2010). The bicelles have a geometry that mimics the plasma membrane, although the lipids that we use are neutral (the inclusion of negatively charged lipids led to unavoidable precipitation of our samples) and are somewhat shorter than those found in mammalian membranes (Chou et al., 2002; Glover et al., 2001).

Nearly all (~98%) of the backbone resonances of the TM-JM construct in the membrane were assigned, using standard TROSY-based double and triple resonance experiments. A detailed description of the NMR analysis is provided in the Extended Experimental Procedures. Briefly, the NMR data for the transmembrane helix are consistent with previous reports describing dimeric structures (Bocharov et al., 2008; Mineev et al., 2010) (Figure 5, Figure S5). In addition, the NMR analysis provides evidence for the formation of a helix by the LRLL motif in the JM-A segment.

We measured intermolecular NOEs between isotopically labeled and unlabeled proteins incorporated into lipid bicelles in two different sets of experiments (Supplementary Experiment Procedures). In total, we measured 285 intramolecular and 21 intermolecular NOE distance restraints (thirteen and eight NOEs for the transmembrane and juxtamembrane segments, respectively; see Tables S1, S2 and Figure S5). While these distance restraints identify the points of contact between the two subunits in the dimer, there are too few to determine the configuration of the TM-JM segment unambiguously. To get around this limitation, we used observations from molecular dynamics simulations of the TM-JM segment in DMPC lipid bilayers (Arkhipov et al.). These simulations indicated that two of the NOE's we observed are likely to arise from a less populated alternative configuration of the transmembrane helix. These NOEs were removed in our determination of the NMR-based model for the TM-JM segment (Figure 5A) (See also Extended Experimental Procedures, Figure S7, Tables S1 and S2).

The dimerization interface utilizes a classical dimerization motif (commonly referred to as a “GxxxG” motif, although the residues represented by G can be any residue with a small sidechain) (Lemmon et al., 1994). The transmembrane helices of the catalytically active members of the EGFR family contain two GxxxG motifs, one at each end of the helix

(Fleishman et al., 2002). EGFR has two overlapping N-terminal GxxxG motifs, resulting in a small-small-x-x-small-small motif, with the small sidechains facing the dimer interface in our structure (Figure 5B). This interface is similar to that observed for Her2 (Bocharov et al., 2008), and is consistent with disulfide crosslinking studies of EGFR (Lu et al., 2010).

The right-handed crossing angle of $\sim -44 \pm 3^\circ$ in our NMR model results in separation of the C-terminal ends of the transmembrane helices by ~ 20 Å, providing the appropriate spacing for the antiparallel interaction between the JM-A helices (Figure 5A). As demonstrated by the intermolecular NOE connectivity, this interface is formed by the sidechains of Leu 655, Leu 658 and Leu 659, located within the LRLL motifs of the two subunits (Figure 5A). These helices interact with each other outside the lipid bilayer, as judged by the NMR-derived water accessibility of the juxtamembrane residues (Figure S5A). The four residues that link the end of the transmembrane helix to the JM-A helix do not have regular secondary structure (Val 650 - Thr 654, see Extended Experimental Procedures and Figure S5).

Disruption of the N-terminal dimerization motif of the transmembrane helix inhibits EGFR activity

The activity of EGFR is insensitive to replacement of essentially any residue in the transmembrane segment by other hydrophobic residues (Lu et al., 2010). We found that EGFR activity is not significantly affected even if two of the interfacial residues in the N-terminal dimerization motif are replaced simultaneously by isoleucine (G625I/A629I, data not shown). In contrast, mutating all four of the small residues in the N-terminal interface to isoleucine (4I, T624I/G625I/G628I/A629I) results in significant inhibition of EGFR, as seen by immunofluorescence and by FACs analysis (Figure 5 C, D). These results, which are also consistent with observations from molecular dynamics simulations (Arkhipov et al.), provide evidence for the importance of the N-terminal association between transmembrane helices in receptor activation.

We also sought to disrupt the N-terminal association of the transmembrane helices by stabilizing interactions through a C-terminal dimerization motif that has been suggested to underlie autoinhibition of the receptor (Fleishman et al., 2002). The replacement of hydrophobic residues in transmembrane helices by glutamate can stabilize helix association because the glutamate sidechain can form intermolecular hydrogen bonds (Sternberg and Gullick, 1989). We

mutated Ile 640, located within the C-terminal dimerization motif, to glutamate. This residue is expected to face the other helix upon dimerization through the C-terminal motif.

We used NMR to examine the effect of this mutation on the TM-JM construct in lipid bicelles. The I640E mutation results in significant chemical shift perturbations throughout the TM-JM construct compared to the wild type (Figure 6A and 6B). In particular, the I640E mutation alters chemical shifts for the C_α atoms of Ala 629 and Ala 637 in the N-terminal and C-terminal dimerization motifs, respectively (Figure 6B). We also observe chemical shift changes in the LRRLL motif in the JM-A segment. The I640E mutation does not perturb the sequential NOE connectivity ($d_{NN(i,i+1)}$) or $^{13}C_\alpha$ secondary-structure induced chemical shifts ($^1C_\alpha$) for the transmembrane helix, suggesting that the mutation does not disrupt the helical nature of this segment (Figure S6).

We measured intermolecular NOEs between labeled and unlabeled TM-JM constructs with the I640E mutation using isotope-filtered NOESY experiments. One of the hallmarks of the N-terminal interface, an NOE between the H_α and H_α atoms of Ala 629 on different helices (Figure S5G), is missing in the I640E mutant, consistent with disruption of the N-terminal interface. Instead, we observe intermolecular NOEs between the H_α and H_α atoms of Ala 637, and between

the H_I atom of Ala 637 and the H_N atom of Gly 639 across the C-terminal interface (Figure 6C).

Thus, dimerization of the transmembrane helices in the I640E mutant brings the residues in the C-terminal dimerization motif into close proximity.

The NMR data indicate that the dimer formed by the I640E mutant is less stable than the wild type dimer (Figure S6C). This is consistent with molecular dynamics simulations of the transmembrane helices with the I640E mutation in lipid bilayers, during which transient dimerization through the C-terminal interface occurs (Arkhipov et al.). Critically, the I640E transmembrane helix never forms a stable dimer through its N-terminal dimerization motif in these simulations.

The NMR data demonstrate that disruption of the N-terminal interface between the transmembrane helices is correlated with disruption of the antiparallel JM-A interaction. We do not observe any sequential NOE connectivity ($d_{NN(i,i+1)}$) or intermolecular NOE connectivity for the juxtamembrane segment in the I640E mutant (Figure S6A), indicating a loss of structure in this region. Molecular dynamics simulations of the TM-JM construct in lipid bicelles also indicate that the formation of a C-terminal transmembrane interface is incompatible with formation of the juxtamembrane dimer interface (Arkhipov et al.).

When we introduce the I640E mutation into the intact receptor, EGF-dependent activation is impaired substantially in comparison to that of the wild type EGFR, particularly at densities below 500 molecules per μm^2 (Figure 6B). Additionally, the constitutive activity of the TM-ICM construct is reduced substantially by introduction of the I640E mutation, as shown by FACS (Figure 6C). These results suggest that interaction of the transmembrane helices through their N-terminal dimerization motif is coupled to formation of an anti-parallel interaction between JM-A helices, both of which are critical for receptor activation

!

Conclusions

Previous work on EGFR led to the conclusion that the presence of the juxtamembrane segment dimerizes the intracellular module in solution, suggesting that the principal function of ligand binding to the intact receptor is to change the structure of the extracellular module such that it does not impede the intrinsic ability of the intracellular module to activate (Jura et al., 2009a). Unexpectedly, we find that ligand binding must play a more direct role in activation, because the intracellular module is monomeric and inhibited when it is localized to the plasma membrane without the transmembrane domain. This suppression of activity at the membrane provides a way for the transmembrane helix to control the intracellular module of EGFR.

Our NMR analysis shows that the formation of the JM-A helix is coupled to the configuration of the transmembrane helices, and that when the JM-A helices interact in an antiparallel manner they do so outside of the membrane. Molecular dynamics simulations suggest that when EGFR is in an inactive conformation, the LRLL motif within the JM-A segment is buried in the membrane (Arkhipov et al.), consistent with NMR data for the isolated

juxtamembrane segment of EGFR in detergent micelles (Choowongkamon et al., 2005). Taken together, these observations suggest a mechanism in which the nature of the interaction between the transmembrane helices toggles the configuration and membrane association of the JM-A portion of the juxtamembrane segments (Figure 7A).

A recent cell-based study on EGFR using a specialized fluorescence reporter clearly links an antiparallel interaction between the JM-A helices to receptor activation and not just dimerization (Scheck et al., 2012). We propose that the JM-A segments need to be pulled off the membrane in order to promote the asymmetric interaction between kinase domains. The latch formed by the JM-B segment of the receiver on the C-lobe of the activator kinase domain positions the sidechain of Glu 666 of the receiver near Arg 949 of the activator, providing an anchor point for the C-terminal end of the receiver JM-A segment (Red Brewer et al., 2009; Wood et al., 2008). In a crystal structure of the EGFR intracellular module with an intact juxtamembrane segment, the JM-A helix is anchored at this point, but is directed away from the surface of the activator kinase by crystal lattice contacts that do not appear to be relevant for activation (Red Brewer et al., 2009). We believe, instead, that the polar face of the JM-A helix of the receiver interacts with the surface of the kinase domain, as modeled earlier (Jura et al., 2009a) and seen consistently in

the molecular dynamics simulations. If the receiver JM-A helix is docked in this way, then the leucine residues of the LRRLL motif point up from the surface of the kinase domain and are available for interaction with the activator JM-A helix, as shown schematically in Figure 7B. Our NMR data suggest that dimerization of the transmembrane helices through the N-terminal interface facilitates this arrangement.

Molecular dynamics simulations indicate that the extracellular module of EGFR prevents the close approach of the transmembrane helices that would be required for interaction through the N-terminal dimerization motif (Arkhipov et al.), even when the receptor is dimerized in the absence of ligand. Consistent with this idea, ligand-independent activation of the receptor can be increased when flexible linkers are inserted between the extracellular module and the transmembrane helix. Thus, we believe that an essential role for EGF in receptor activation is to cause a specific conformational change in the extracellular modules that allows the transmembrane helices to interact through their N-terminal interface.

A striking feature of the activation mechanism is the strong cooperativity between the external, internal and transmembrane segments of EGFR as the receptor transitions from an inhibited to an activated state upon ligand binding. We speculate that because the EGFR dimer

interface is mediated entirely by the receptor itself, selective pressure for inhibitory mechanisms to prevent ligand-independent activation has been particularly strong. At the same time, because EGFR signaling requires a specific arrangement of kinase domains, the selective stabilization of a particular dimeric configuration is important for activation. The balance of these competing requirements may have driven the evolution of counter-balanced activating and inhibiting mechanisms that prevent ligand-independent activation and facilitate the formation of appropriate heterodimers in response to external cues.

Experimental Procedures

Mammalian Cell-Based Assays

For immunofluorescence experiments, Cos-7 cells were grown on etched glass coverslips, transfected with Fugene (Promega) and serum-starved. When noted, cells were treated with EGF (100 ng/ml, PeproTech) for 3 minutes at 37°C. After fixation in 2% formaldehyde, permeabilization with 0.1% triton X-100, and blocking with 0.2% bovine serum albumin (BSA), cells were stained with Y1068 primary antibody then anti-rabbit fluorescein-labeled (FITC) antibody (Sigma). Cells were mounted with Thermomount (Thermo Scientific) with 0.2% trans-pyridine-2-azo-p-dimethylaniline (Sigma) for immunofluorescence, or with Prolong Gold (Invitrogen) for confocal imaging. For live and confocal imaging cells were grown in glass bottom dishes (Matek). Samples for flow cytometry were prepared similarly to immunofluorescence microscopy (Experimental Procedures) with an additional step of dissociating cells with trypsin before fixation. More details can be found in the Extended Experimental Procedures.

Analysis of phosphorylation as a function of expression level

Cells were imaged with a TE-2000 Nikon fluorescence microscope with a xenon lamp (Nikon Instruments Inc.) through a 60x TIRF objective and standard filter sets (Chroma) using a CoolSnap CCD camera (Photometrics). The microscope was calibrated for mCherry intensity using lipid bilayers containing Texas-Red lipids and mCherry purified from *E. coli* as described (Galush et al., 2008). For each cell the mean value for both mCherry intensity and FITC intensity were measure in selected regions in the cell periphery and corrected for background using ImageJ software (Schneider et al., 2012). Calculation of the phosphorylation level per receptor included correction for background phosphorylation levels in cells expressing low levels of EGFR (less than 100 molecules per μm^2), and normalization to EGFR levels for samples fixed on the same day. More details on both instrumentation and analysis for microscopy and FACS experiments are provided in the Extended Experimental Procedures.

Fluorescence correlation spectroscopy

Fluorescence correlation spectroscopy was performed on a custom modified inverted microscope (Nikon Eclipse Ti, Nikon Instruments Inc). Briefly, a 200 fs pulsed, 560 nm laser beam was synced with a 100 ps pulsed, 482 nm diode laser and delayed by 50 ns. Both lasers

were coupled into a single mode optical fiber and then collimated to a 4 mm beam diameter. Samples were excited through a 100x objective (CFI APO 100X Oil TIRF NA 1.49, Nikon Instruments Inc.), with laser powers of $\sim 1\mu\text{W}$ measured before the objective. Fluorescence emitted from the sample is directed to a long wave pass dichroic beamsplitter (FF562-Di02-25x36, Semrock Inc.) and on to a pair of bandpass filtered single photon avalanche diodes (PDM module, Optoelectronic Components). Detector output was measured with a time-correlated single photon counting module (PicoHarp 300, PicoQuant Photonics Inc), with a time resolution of 32 ps. More details on the light sources and path are discussed in the Extended Experimental Procedures.

Each detected photon is tagged with its absolute arrival time, and the delay time with respect to the laser pulses. Photons are collated into 10 μs time bins after being sorted by detector channel and arrival time. This generates a time-dependent fluorescence signal, free from green to red bleed-through, FRET, and direct mCherry excitation by the 482 nm laser. Fluorescence correlation and cross-correlation spectra are calculated as described (Extended Experimental Procedures).

NMR Spectroscopy

The transmembrane-juxtamembrane segment (TM-JM, residues 618 – 673) of EGFR was purified from inclusion bodies as discussed in the Extended Experimental Procedures. The NMR sample was prepared by dissolving the purified protein in deuterated TFE and then mixing with deuterated DMPC and DHPC lipids (Avanti Polar Lipids, Inc). The protein and the lipids were mixed in a ratio of 1:150 and the DMPC to DHPC ratio was set at 0.25. The final NMR sample (at a protein concentration of 0.3 mM) was prepared by resuspending the protein and the lipid mixture in a sample buffer containing 50 mM MES pH 6.2, 5 mM TCEP, 1 mM EDTA, 0.05 mM ABESF, 7% $^2\text{H}_2\text{O}$, 0.02% NaN_3 .

All NMR experiments were performed at ^1H frequencies of 600 MHz or 900 MHz on Bruker Avance spectrometers fitted with TCI cryo-probes. The backbone chemical shift assignments were obtained through TROSY-based triple resonance experiments (Kay et al., 1990; Pervushin et al., 1997; Salzmann et al., 1998). Intermolecular NOEs were resolved by 3D ^{15}N - ^{13}C F1-filtered/F3-edited NOESY-HSQC and methyl ^{13}C -edited NOESY-HSQC experiments (Breeze, 2000; Stuart et al., 1999). The backbone amide resonances for the I640E mutant were assigned using TROSY HNCA, ^{13}C (CT)-HSQC spectra and 3D NOESY experiments. The structural model for the TM-JM dimer was generated using the simulated annealing protocol of

CNS (v1.3) (Brunger, 2007). A detail description of the NMR methods and structure calculation is provided in the Extended Experimental Procedures.

Figure 1. Model for EGFR Activation and Domain Architecture

- (A) Model for monomer-dimer equilibrium of EGFR in the absence and presence of EGF (Yarden and Schlessinger, 1987).
- (B) EGFR constructs used in this study.

Figure 2. Surface-Density Dependence of EGFR Activation (See also Figure S1)!

- (A) Cos-7 cells viewed by fluorescence microscopy, expressing EGFR fused to mCherry (left column, red) with phosphorylation at Tyr 1068 (pY1068) detected using a fluorescein-labeled antibody (middle column, green, Experimental Procedures). Expression and phosphorylation channels are merged in the right column. Top row, before EGF stimulation. Bottom row, after stimulation with EGF for 3 minutes at 37°C.
- (B) Relationship between EGFR surface density and phosphorylation level, determined from images such as those shown in Figure 2A. Individual data points in the left panel represent the mean surface density and the mean fluorescence intensity from the pY1068 antibody (arbitrary units) in selected regions, average in bins of cells containing cells with comparable surface

density (within 100 molecules per μm^2 of the mean value). Trend lines were calculated using linear and second-order polynomial fits for EGFR with and without ligand, respectively. In the right panel, bars represent the mean ratio of phosphorylation intensity to surface density for all cells within equal ranges of surface densities (value on x-axis ± 250 molecules per μm^2). In these diagrams, as well as all subsequent ones, error bars represent the standard error of the mean.

(C) Surface density-dependent phosphorylation for a construct with extracellular domain deleted (TM-ICM) compared to EGFR \pm EGF.

(D) Surface density-dependent phosphorylation levels for a construct with a flexible linker inserted between the extracellular module and the transmembrane (ECM-GlySer-TMICM) compared to EGFR.

Figure 3. Activity of the Intracellular Module Localized to the Plasma Membrane with the c-Src Motif (See also Figures S2 and S3)

(A) Confocal images of cells expressing EGFR (top panels) and the intracellular module with the c-Src membrane localization motif (Myr-ICM, bottom panels), with antibody detection of

phosphorylation at pY1068. Expression is shown in left panels, phosphorylation level in middle panels and the merged intensities in the right panel. The large boxes are views in the x-y plane of the basal surface of the cells (closest to the coverslip). The small boxes underneath are projections in the x-z plane, orthogonal to the basal surface, at the y-coordinate indicated by the white arrow.

(B) Surface-density dependence of phosphorylation for Myr-ICM compared to EGF-treated EGFR and Myr-GCN4-ICM.

(C) Schematic model for docking of the EGFR kinase domain against the plasma membrane based on molecular dynamics simulations of unliganded EGFR in lipid bilayers (Arkhipov et al.). Dashed boxes highlight three regions of interaction between the intracellular module and the membrane. In the kinase domain, positively charged residues that interact with negative charged lipids during the simulations are labeled and shown as blue dots. The LRRL motif in the juxtamembrane-A segment is shown in stick form, with leucines in green and arginines in blue.

(D) Surface-density dependence of phosphorylation for charge reversal mutations in the N-lobe interaction region of the intracellular domain (Myr-ICM K713E/K715E), compared to Myr-ICM and EGF-treated EGFR.

(E) Surface-density dependence of phosphorylation for another set of charge reversal mutations in the N-lobe (Myr-ICM K689E/K692E), compared to Myr-ICM and EGF-treated EGFR. These data were collected on the same day as in Figure 3D.

(F) Surface-density dependence of phosphorylation for ECM-TM-GlySer-ICM and EGFR in the absence and presence of EGF.

Figure 4. Fluorescence Cross-Correlation Spectroscopy Data for EGFR Constructs on the Plasma Membrane (See also Figure S4)

(A) Schematic of laser excitation and fluorescence detection for two-color pulsed interleaved excitation fluorescence cross-correlation spectroscopy (PIE-FCCS, left). Pulse diagram (right) showing excitation pulses (top panel, with GFP in blue and mCherry in green) and emission (bottom panel, with GFP in green and mCherry in red). Note that time gating allows us to eliminate mCherry emission when GFP is excited.

(B) Relative cross-correlation values for various EGFR constructs. Myr-FP is a coexpression of GFP and mCherry each fused separately to the c-Src membrane localization motif. Data are represented as a scatter plot, with the red line representing the median value. Surface densities of EGFR constructs ranged from 100 - 1000 molecules per μm^2 .

Figure 5. NMR Structure of Transmembrane-Juxtamembrane Dimer in Bicelles and Effect of the I640E Mutation on Receptor Activation (See also Figure S5 and S7)

(A) Structural model of the transmembrane-juxtamembrane segment of EGFR in DMPC/DHPC bicelles as determined from NMR data. Intermolecular NOESY connectivities are shown with grey lines. The dimer interfaces are shown in the right panels.

(B) Expanded view of transmembrane dimer interface with small-small-x-x-small-small motif highlighted.

(C) Surface-density dependence of phosphorylation for EGFR with four residues in the N-interface mutated (4I, T624I/G625I/G628I/A629I). Both wildtype and mutant EGFR are compared with or without EGF treatment.

(D) FACS data comparing EGFR expression level (x-axis) to pY1068 level for wildtype EGFR and the 4I mutant.

Figure 6. The Effect of the I640E Mutation on Transmembrane Helix Structure (See also Figure S6)

(A) ^1H , ^{15}N chemical shift differences between the I640E mutant and the wildtype TM-JM segment for each residue. The solid (red) and dashed (black) horizontal lines represent the chemical shift differences expected based on the digital resolution of the spectra and calculated from the average chemical shift, respectively. The vertical red dashed lines represent the predicted membrane-spanning region, based on the sequence analysis.

(B) The Ala C_α region from the ^1H - ^{13}C (CT) HSQC spectra of the wildtype and I640E TM-JM segments in DMPC/DHPC bicelles, respectively. Schematic representation of the C-terminal dimer is shown at the right, with the uniformly labeled helix on the left and unlabeled one on the right. Residues in close proximity in the I640E mutant are shown as green and blue circles on the labeled and unlabeled helices, respectively. Alanine residues shown as red circles do not show NOE connectivity in the I640E mutant.

(C) Representative 2D strip plot showing the Ala 637 H_α intermolecular NOE cross peak at the ^{13}C frequency of Ala 637 C_α , from 3D ^{15}N - ^{13}C F1-filtered/F3-edited NOESY-HSQC spectra. Close contacts between residues showing intermolecular NOEs in this panel are observed in the molecular dynamics simulations of the I640E mutant (Arkhipov et al.).

(D) Surface-density dependence of phosphorylation for EGFR with a mutation designed to destabilize the dimer interface observed in 5A (I640E, see also Figure 6). Both wildtype and mutant EGFR are compared with or without EGF treatment.

(E) FACS data comparing expression level (x-axis) to pY1068 level for the TM-ICM construct, with or without the I640E mutation.

Figure 7. Model for Structural Coupling Between the Transmembrane helices and the Intracellular Modules

(A) Model for structural coupling between the transmembrane helices and the juxtamembrane segments (JM-A) at the plasma membrane, based on NMR data and molecular dynamics simulations (Arkhipov et al.). The LRLL motif in JM-A is highlighted, with leucine and arginine sidechains in green and blue, respectively.

(B) Model for asymmetric dimer formation at the plasma membrane. The surface of the kinase domains and the backbone of the juxtamembrane segments are shown in green and blue for the two molecules in the dimer, respectively. Residues in the LRLL motif in the JMA are shown as

sticks, with leucine in yellow (activator) or green (receiver) and arginine in blue. Glu 666 of the receiver and Arg 949 of the activator are indicated by red and blue circles respectively.

- Alvarado, D., Klein, D.E., and Lemmon, M.A. (2010). Structural basis for negative cooperativity in growth factor binding to an EGF receptor. *Cell* 142, 568-579.
- Becker, W., Bergmann, A., Geddes, C.D., and Lakowicz, J.R. (2005). Multi-Dimensional Time-Correlated Single Photon Counting, Vol 2005 (Springer US).
- Bocharov, E.V., Mineev, K.S., Volynsky, P.E., Ermolyuk, Y.S., Tkach, E.N., Sobol, A.G., Chupin, V.V., Kirpichnikov, M.P., Efremov, R.G., and Arseniev, A.S. (2008). Spatial structure of the dimeric transmembrane domain of the growth factor receptor ErbB2 presumably corresponding to the receptor active state. *J Biol Chem* 283, 6950-6956.
- Breeze, A.L. (2000). Isotope-filtered NMR methods for the study of biomolecular structure and interactions. *Prog Nucl Mag Res Sp* 36, 323-372.
- Brunger, A.T. (2007). Version 1.2 of the Crystallography and NMR system. *Nat Protoc* 2, 2728-2733.
- Chantry, A. (1995). The kinase domain and membrane localization determine intracellular interactions between epidermal growth factor receptors. *J Biol Chem* 270, 3068-3073.
- Choowongkamon, K., Carlin, C.R., and Sonnichsen, F.D. (2005). A structural model for the membrane-bound form of the juxtamembrane domain of the epidermal growth factor receptor. *J Biol Chem* 280, 24043-24052.
- Chou, J.J., Kaufman, J.D., Stahl, S.J., Wingfield, P.T., and Bax, A. (2002). Micelle-induced curvature in a water-insoluble HIV-1 Env peptide revealed by NMR dipolar coupling measurement in stretched polyacrylamide gel. *J Am Chem Soc* 124, 2450-2451.
- Clayton, A.H., Orchard, S.G., Nice, E.C., Posner, R.G., and Burgess, A.W. (2008). Predominance of activated EGFR higher-order oligomers on the cell surface. *Growth Factors* 26, 316-324.
- Cohen, P. (2002). Protein kinases--the major drug targets of the twenty-first century? *Nat Rev Drug Discov* 1, 309-315.
- Ferguson, K.M., Berger, M.B., Mendrola, J.M., Cho, H.S., Leahy, D.J., and Lemmon, M.A. (2003). EGF activates its receptor by removing interactions that autoinhibit ectodomain dimerization. *Mol Cell* 11, 507-517.
- Fleishman, S.J., Schlessinger, J., and Ben-Tal, N. (2002). A putative molecular-activation switch in the transmembrane domain of erbB2. *Proc Natl Acad Sci U S A* 99, 15937-15940.
- Galush, W.J., Nye, J.A., and Groves, J.T. (2008). Quantitative fluorescence microscopy using supported lipid bilayer standards. *Biophys J* 95, 2512-2519.
- Garrett, T.P., McKern, N.M., Lou, M., Elleman, T.C., Adams, T.E., Lovrecz, G.O., Zhu, H.J., Walker, F., Frenkel, M.J., Hoyne, P.A., *et al.* (2002). Crystal structure of a truncated epidermal

- growth factor receptor extracellular domain bound to transforming growth factor alpha. *Cell* **110**, 763-773.
- Glover, K.J., Whiles, J.A., Wu, G., Yu, N., Deems, R., Struppe, J.O., Stark, R.E., Komives, E.A., and Vold, R.R. (2001). Structural evaluation of phospholipid bicelles for solution-state studies of membrane-associated biomolecules. *Biophys J* **81**, 2163-2171.
- Haigler, H., Ash, J.F., Singer, S.J., and Cohen, S. (1978). Visualization by fluorescence of the binding and internalization of epidermal growth factor in human carcinoma cells A-431. *Proc Natl Acad Sci U S A* **75**, 3317-3321.
- Hubbard, S.R., and Till, J.H. (2000). Protein tyrosine kinase structure and function. *Annu Rev Biochem* **69**, 373-398.
- Hynes, N.E., and Lane, H.A. (2005). ERBB receptors and cancer: the complexity of targeted inhibitors. *Nat Rev Cancer* **5**, 341-354.
- Jura, N., Endres, N.F., Engel, K., Deindl, S., Das, R., Lamers, M.H., Wemmer, D.E., Zhang, X., and Kuriyan, J. (2009a). Mechanism for activation of the EGF receptor catalytic domain by the juxtamembrane segment. *Cell* **137**, 1293-1307.
- Jura, N., Shan, Y., Cao, X., Shaw, D.E., and Kuriyan, J. (2009b). Structural analysis of the catalytically inactive kinase domain of the human EGF receptor 3. *Proc Natl Acad Sci U S A* **106**, 21608-21613.
- Kay, L.E., Ikura, M., Tschudin, R., and Bax, A. (1990). 3-Dimensional Triple-Resonance Nmr-Spectroscopy of Isotopically Enriched Proteins. *J Magn Reson* **89**, 496-514.
- Larson, D.R., Gosse, J.A., Holowka, D.A., Baird, B.A., and Webb, W.W. (2005). Temporally resolved interactions between antigen-stimulated IgE receptors and Lyn kinase on living cells. *J Cell Biol* **171**, 527-536.
- Lemmon, M.A., and Schlessinger, J. (2010). Cell signaling by receptor tyrosine kinases. *Cell* **141**, 1117-1134.
- Lemmon, M.A., Treutlein, H.R., Adams, P.D., Brunger, A.T., and Engelman, D.M. (1994). A dimerization motif for transmembrane alpha-helices. *Nat Struct Biol* **1**, 157-163.
- Liu, P., Cleveland, T.E., Bouyain, S., Byrne, P.O., Longo, P.A., and Leahy, D.J. (2012). A single ligand is sufficient to activate EGFR dimers. *Proc Natl Acad Sci U S A*.
- Lu, C., Mi, L.Z., Grey, M.J., Zhu, J., Graef, E., Yokoyama, S., and Springer, T.A. (2010). Structural evidence for loose linkage between ligand binding and kinase activation in the epidermal growth factor receptor. *Mol Cell Biol* **30**, 5432-5443.
- Macdonald, J.L., and Pike, L.J. (2008). Heterogeneity in EGF-binding affinities arises from negative cooperativity in an aggregating system. *Proc Natl Acad Sci U S A* **105**, 112-117.
- McLaughlin, S., Smith, S.O., Hayman, M.J., and Murray, D. (2005). An electrostatic engine model for autoinhibition and activation of the epidermal growth factor receptor (EGFR/ErbB) family. *J Gen Physiol* **126**, 41-53.
- Mineev, K.S., Bocharov, E.V., Pustovalova, Y.E., Bocharova, O.V., Chupin, V.V., and Arseniev, A.S. (2010). Spatial structure of the transmembrane domain heterodimer of ErbB1 and ErbB2 receptor tyrosine kinases. *J Mol Biol* **400**, 231-243.
- Moriki, T., Maruyama, H., and Maruyama, I.N. (2001). Activation of preformed EGF receptor dimers by ligand-induced rotation of the transmembrane domain. *J Mol Biol* **311**, 1011-1026.
- Muller, B.K., Zaychikov, E., Brauchle, C., and Lamb, D.C. (2005). Pulsed interleaved excitation. *Biophys J* **89**, 3508-3522.

- Nagy, P., Claus, J., Jovin, T.M., and Arndt-Jovin, D.J. (2010). Distribution of resting and ligand-bound ErbB1 and ErbB2 receptor tyrosine kinases in living cells using number and brightness analysis. *Proc Natl Acad Sci U S A* *107*, 16524-16529.
- Nishikawa, R., Ji, X.D., Harmon, R.C., Lazar, C.S., Gill, G.N., Cavenee, W.K., and Huang, H.J. (1994). A mutant epidermal growth factor receptor common in human glioma confers enhanced tumorigenicity. *Proc Natl Acad Sci U S A* *91*, 7727-7731.
- O'Shea, E.K., Klemm, J.D., Kim, P.S., and Alber, T. (1991). X-ray structure of the GCN4 leucine zipper, a two-stranded, parallel coiled coil. *Science* *254*, 539-544.
- Ogiso, H., Ishitani, R., Nureki, O., Fukai, S., Yamanaka, M., Kim, J.H., Saito, K., Sakamoto, A., Inoue, M., Shirouzu, M., *et al.* (2002). Crystal structure of the complex of human epidermal growth factor and receptor extracellular domains. *Cell* *110*, 775-787.
- Pervushin, K., Riek, R., Wider, G., and Wuthrich, K. (1997). Attenuated T2 relaxation by mutual cancellation of dipole-dipole coupling and chemical shift anisotropy indicates an avenue to NMR structures of very large biological macromolecules in solution. *Proc Natl Acad Sci U S A* *94*, 12366-12371.
- Qiu, C., Tarrant, M.K., Choi, S.H., Sathyamurthy, A., Bose, R., Banjade, S., Pal, A., Bornmann, W.G., Lemmon, M.A., Cole, P.A., *et al.* (2008). Mechanism of activation and inhibition of the HER4/ErbB4 kinase. *Structure* *16*, 460-467.
- Red Brewer, M., Choi, S.H., Alvarado, D., Moravcevic, K., Pozzi, A., Lemmon, M.A., and Carpenter, G. (2009). The juxtamembrane region of the EGF receptor functions as an activation domain. *Mol Cell* *34*, 641-651.
- Reuther, G.W., Buss, J.E., Quilliam, L.A., Clark, G.J., and Der, C.J. (2000). Analysis of function and regulation of proteins that mediate signal transduction by use of lipid-modified plasma membrane-targeting sequences. *Methods Enzymol* *327*, 331-350.
- Salzmann, M., Pervushin, K., Wider, G., Senn, H., and Wuthrich, K. (1998). TROSY in triple-resonance experiments: new perspectives for sequential NMR assignment of large proteins. *Proc Natl Acad Sci U S A* *95*, 13585-13590.
- Scheck, R.A., Lowder, M.A., Appelbaum, J.S., and Schepartz, A. (2012). Bipartite Tetracysteine Display Reveals Allosteric Control of Ligand-Specific EGFR Activation. *ACS Chem Biol*.
- Schneider, C.A., Rasband, W.S., and Eliceiri, K.W. (2012). NIH Image to ImageJ: 25 years of image analysis. *Nature Methods* *9*, 671-675.
- Scott, J.D., and Pawson, T. (2009). Cell signaling in space and time: where proteins come together and when they're apart. *Science* *326*, 1220-1224.
- Shi, F., Telesco, S.E., Liu, Y., Radhakrishnan, R., and Lemmon, M.A. (2010). ErbB3/HER3 intracellular domain is competent to bind ATP and catalyze autophosphorylation. *Proc Natl Acad Sci U S A* *107*, 7692-7697.
- Silverman, L., and Resh, M.D. (1992). Lysine residues form an integral component of a novel NH2-terminal membrane targeting motif for myristylated pp60v-src. *J Cell Biol* *119*, 415-425.
- Sorkin, A., and Goh, L.K. (2009). Endocytosis and intracellular trafficking of ErbBs. *Exp Cell Res* *315*, 683-696.
- Sorokin, A. (1995). Activation of the EGF receptor by insertional mutations in its juxtamembrane regions. *Oncogene* *11*, 1531-1540.
- Sternberg, M.J., and Gullick, W.J. (1989). Neu receptor dimerization. *Nature* *339*, 587.
- Stuart, A.C., Borzilleri, K.A., Withka, J.M., and Palmer, A.G. (1999). Compensating for variations in H-1-C-13 scalar coupling constants in isotope-filtered NMR experiments. *Journal of the American Chemical Society* *121*, 5346-5347.

- Thiel, K.W., and Carpenter, G. (2007). Epidermal growth factor receptor juxtamembrane region regulates allosteric tyrosine kinase activation. *Proc Natl Acad Sci U S A* *104*, 19238-19243.
- Wallasch, C., Weiss, F.U., Niederfellner, G., Jallal, B., Issing, W., and Ullrich, A. (1995). Heregulin-dependent regulation of HER2/neu oncogenic signaling by heterodimerization with HER3. *EMBO J* *14*, 4267-4275.
- Wood, E.R., Shewchuk, L.M., Ellis, B., Brignola, P., Brashear, R.L., Caferro, T.R., Dickerson, S.H., Dickson, H.D., Donaldson, K.H., Gaul, M., *et al.* (2008). 6-Ethynylthieno[3,2-d]- and 6-ethynylthieno[2,3-d]pyrimidin-4-anilines as tunable covalent modifiers of ErbB kinases. *Proc Natl Acad Sci U S A* *105*, 2773-2778.
- Yarden, Y., and Schlessinger, J. (1987). Self-phosphorylation of epidermal growth factor receptor: evidence for a model of intermolecular allosteric activation. *Biochemistry* *26*, 1434-1442.
- Zhang, X., Gureasko, J., Shen, K., Cole, P.A., and Kuriyan, J. (2006). An allosteric mechanism for activation of the kinase domain of epidermal growth factor receptor. *Cell* *125*, 1137-1149.
- Zhu, H.J., Iaria, J., Orchard, S., Walker, F., and Burgess, A.W. (2003). Epidermal growth factor receptor: association of extracellular domain negatively regulates intracellular kinase activation in the absence of ligand. *Growth Factors* *21*, 15-30.

This manuscript has been authored by an author at Lawrence Berkeley National Laboratory under Contract No. DE-AC02-05CH112321 with the U.S. Department of Energy. The U.S. Government retains, and the publisher, by accepting the article for publication, acknowledges, that the U.S. Government retains a non-exclusive, paid-up irrevocable, world-wide license to publish or reproduce the published form of this manuscript, or allow others to do so, for U.S. Government purposed.

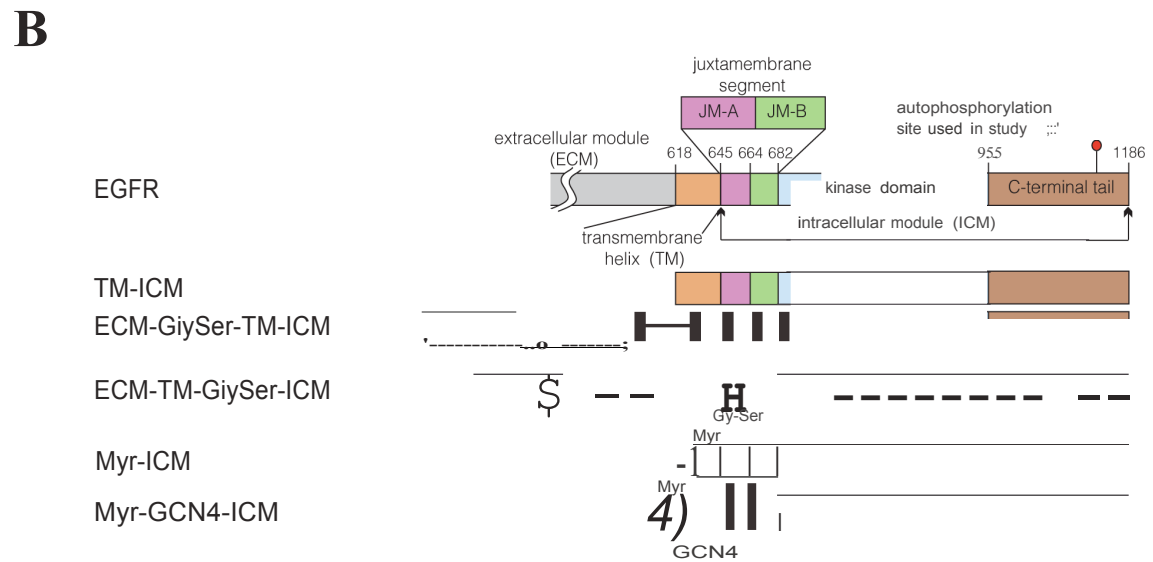
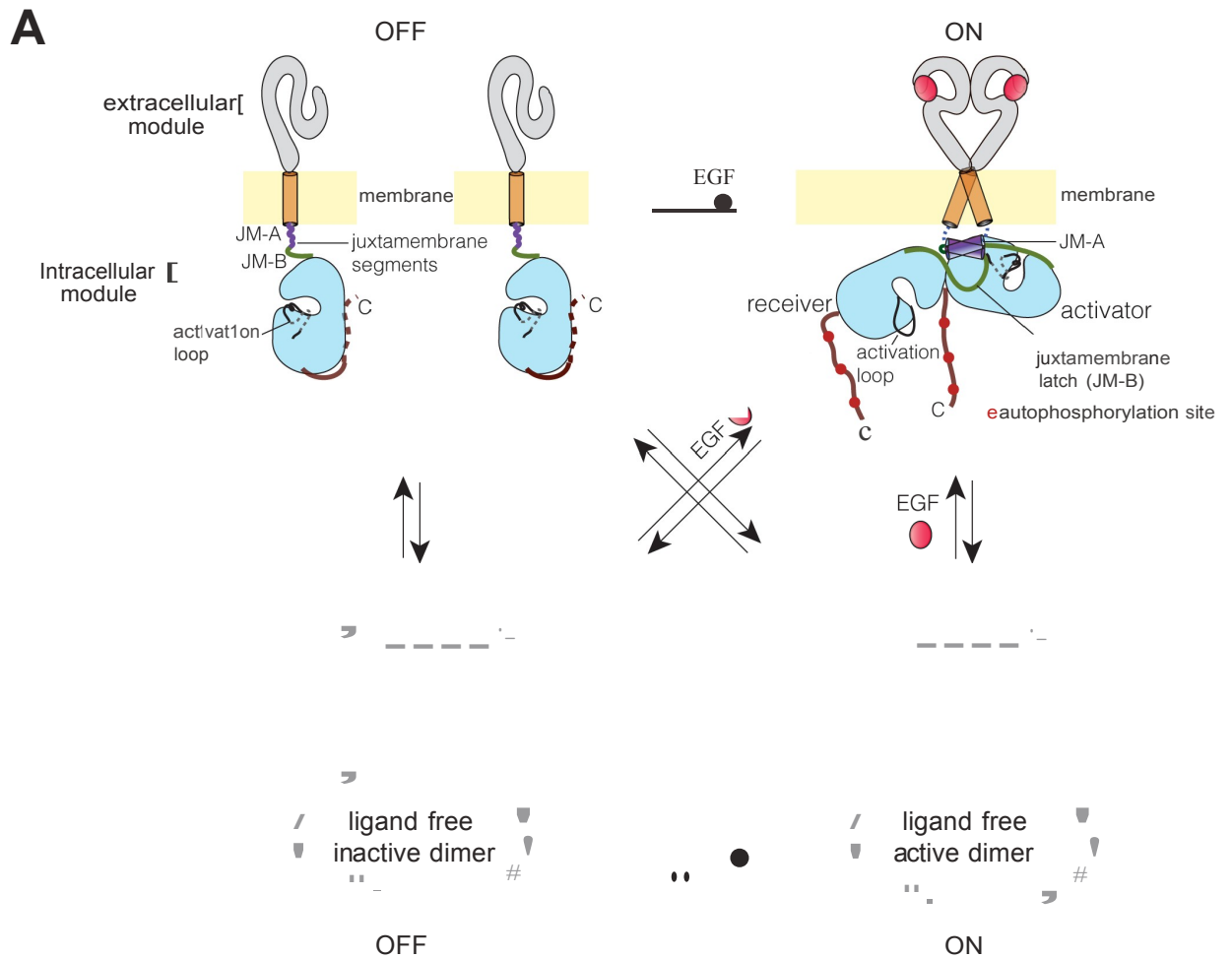


Figure 1

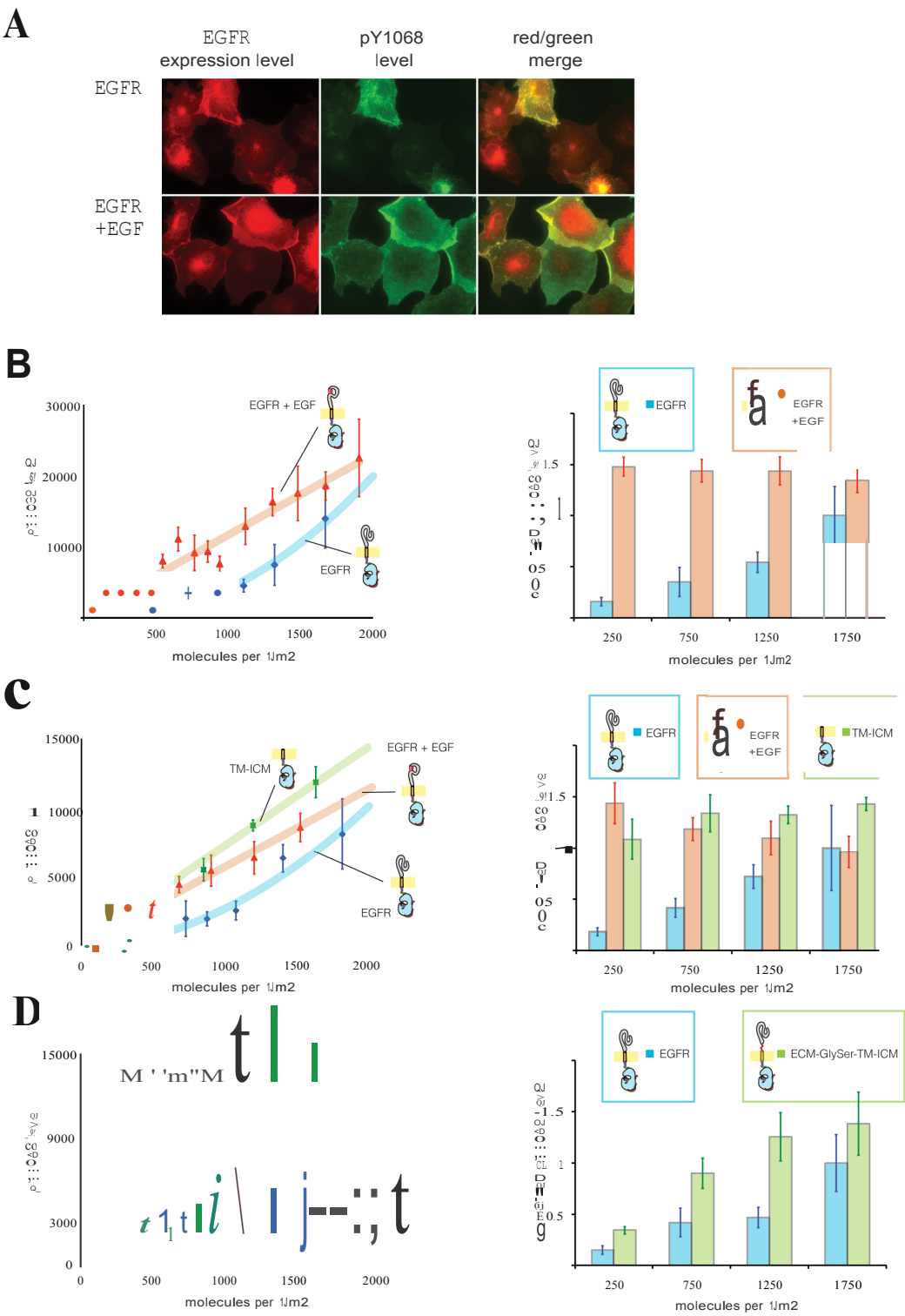
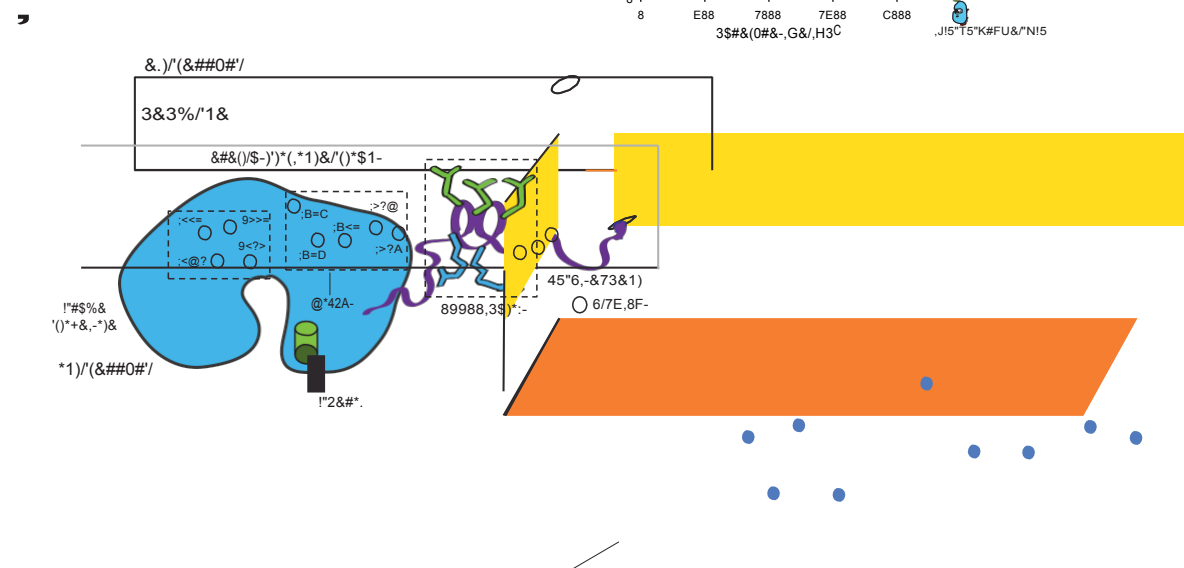
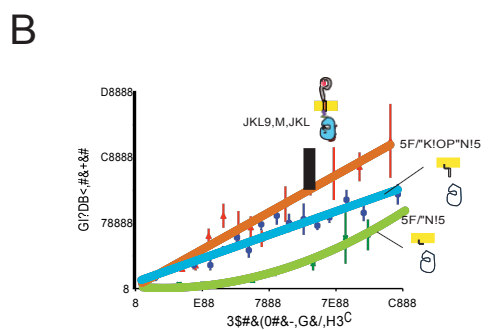
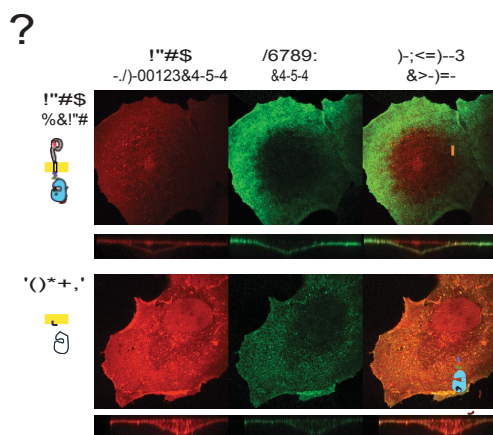
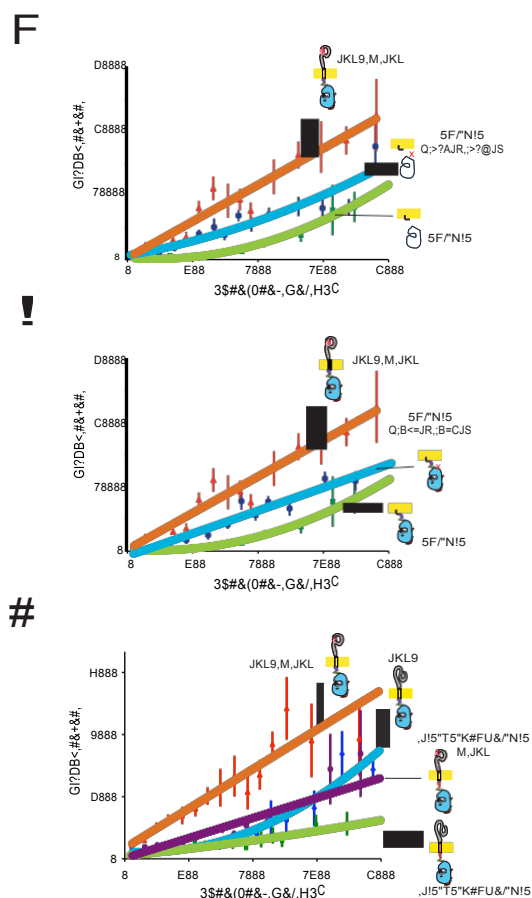


Figure 2



#1=G)-&D



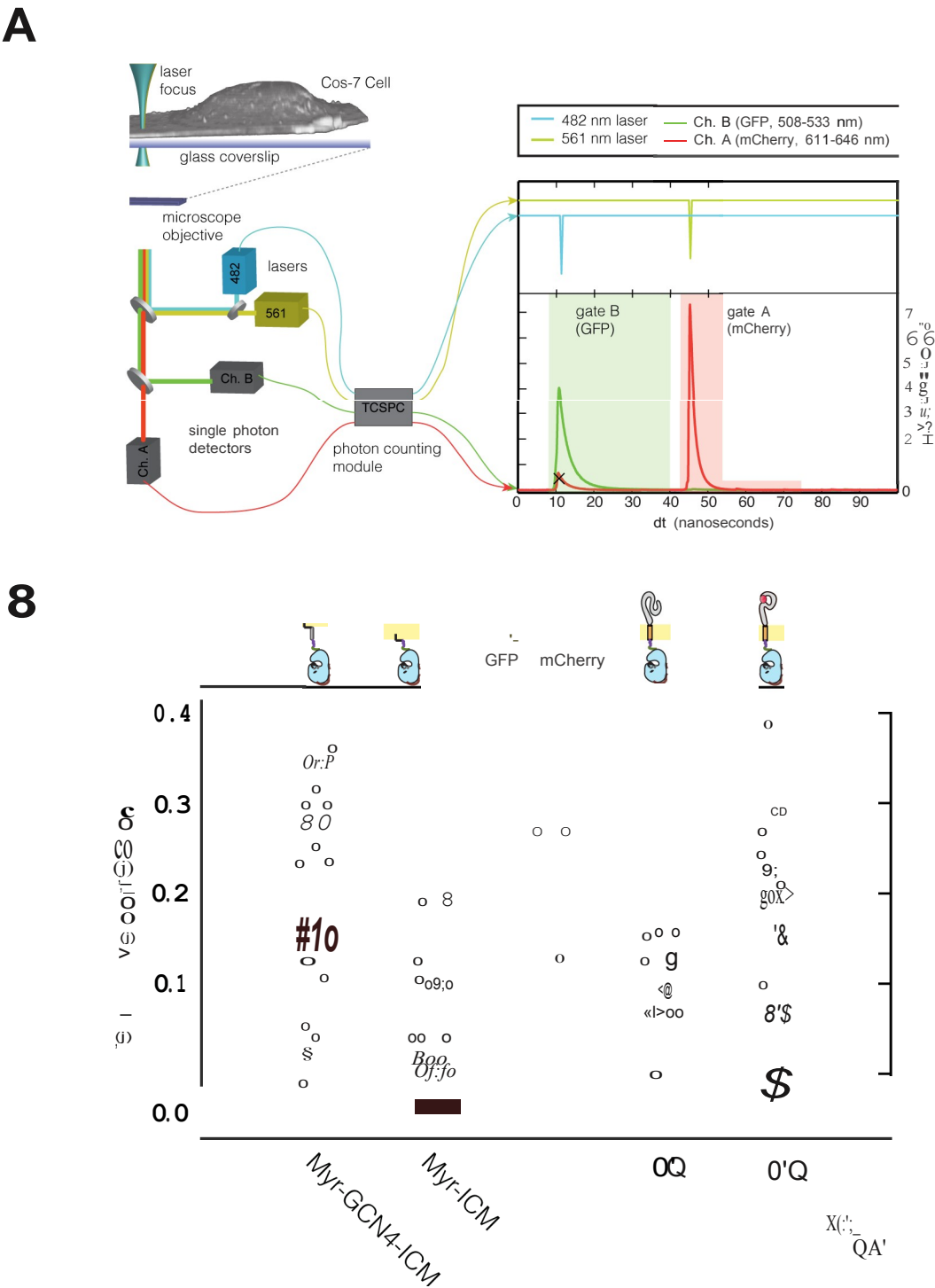
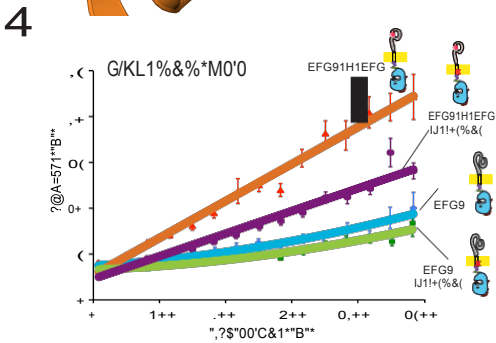
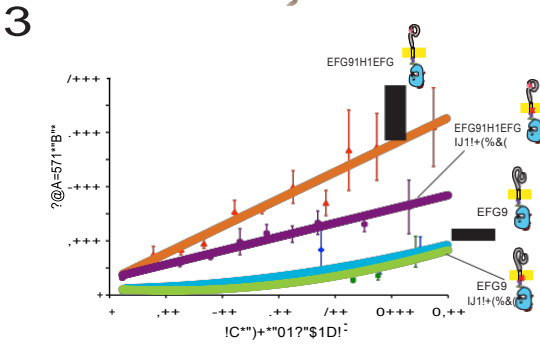
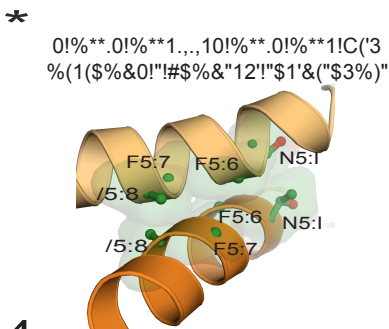
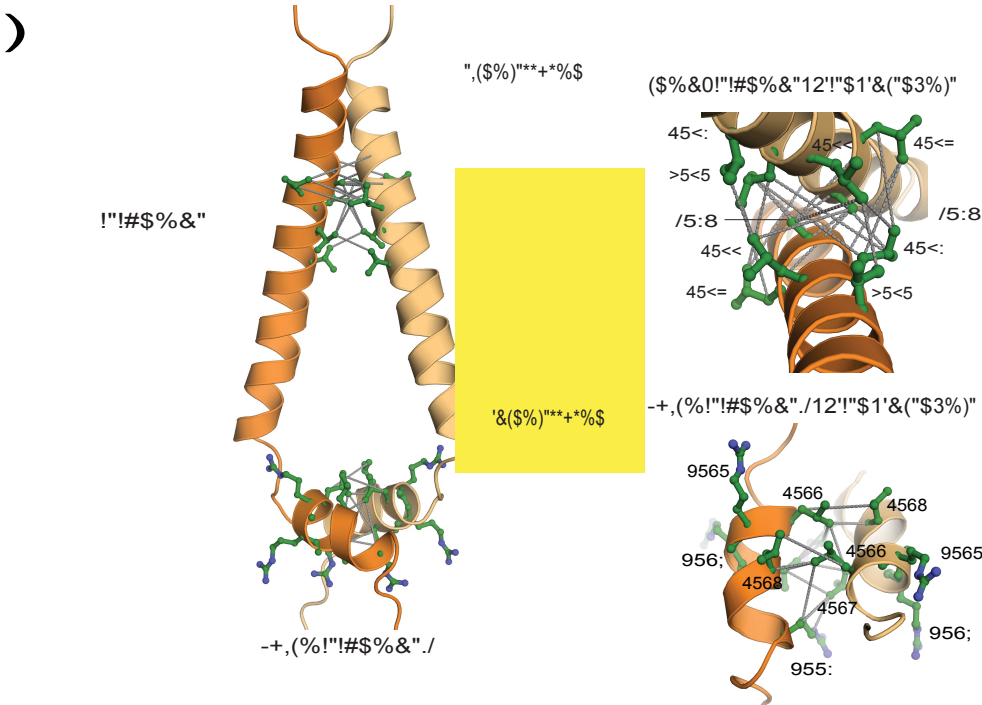


Figure 4



! "#\$%&'(

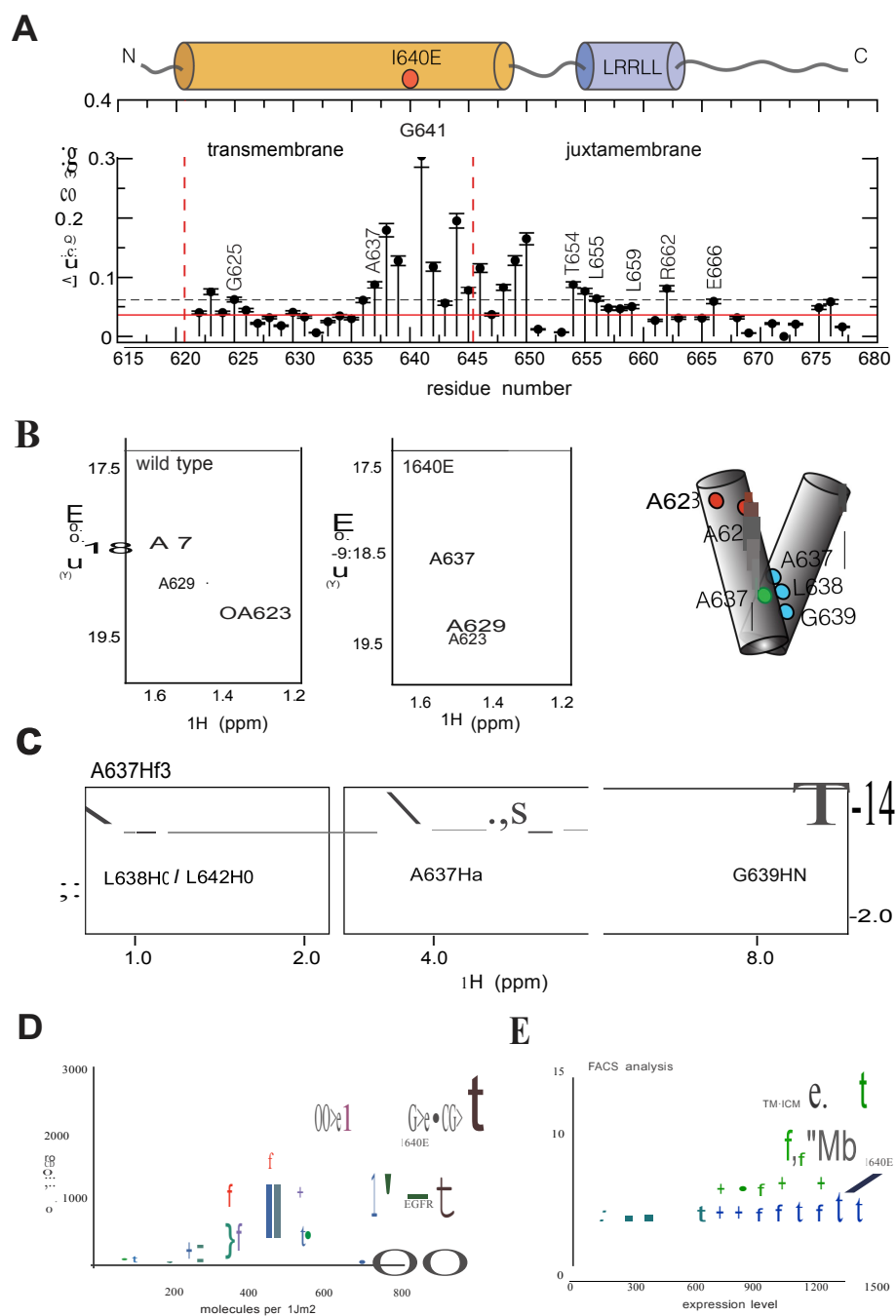


Figure 6

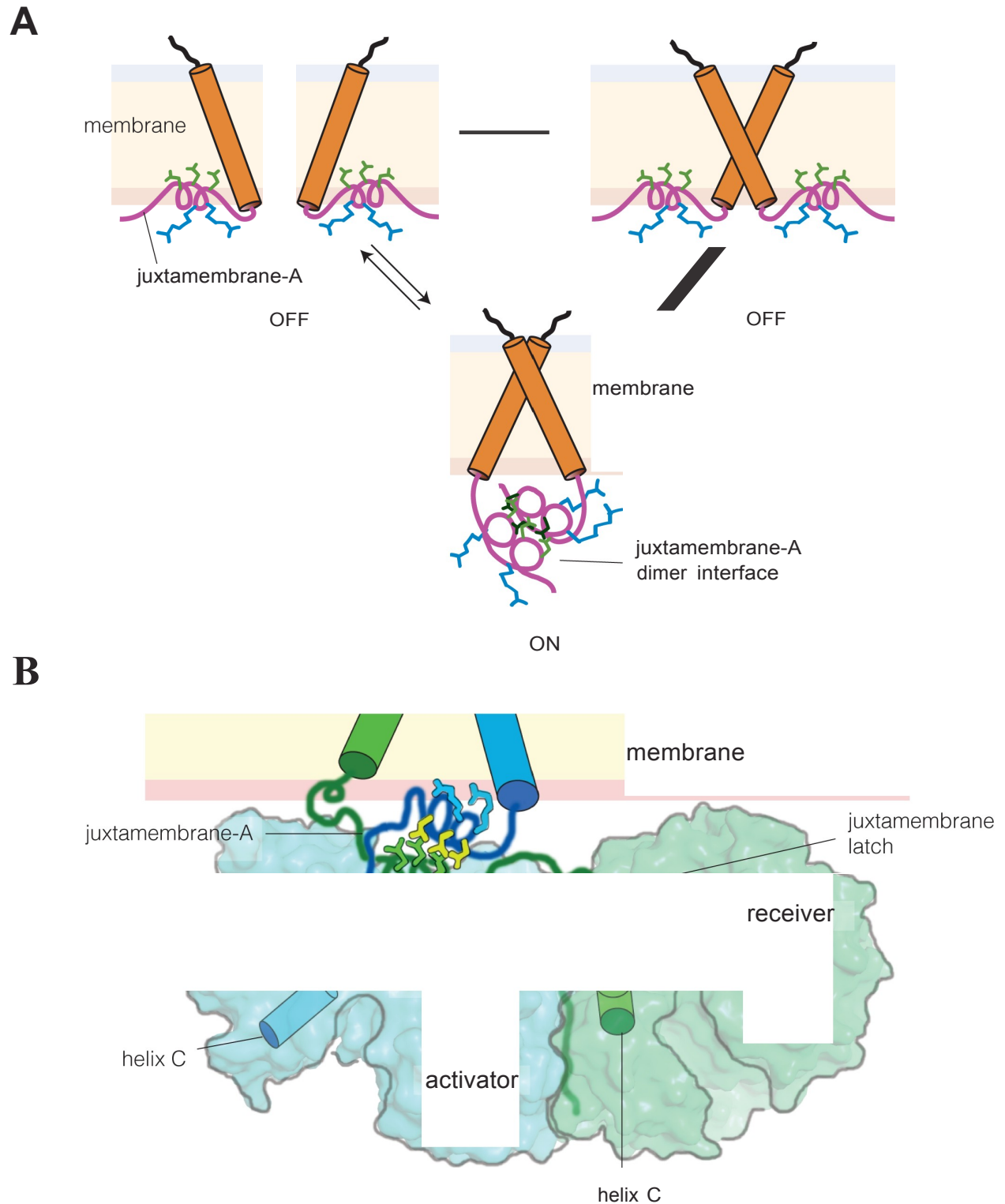


Figure 7